International Journal of Nanoelectronics and Materials

In Press, Accepted Manuscript – Note to user

Nano Hydroxyapatite (Nano-HA) Based on Pholas Orientalis Shells and Degradation Analysis

Mohd Riza Mohd Roslan[1], Nashrul Fazli Mohd Nasir[1,2], Nur Farahiyah Mohammad[1,2], Farah Diana Mohd Daud[3], Cheng Ee Meng[1] and Beh Chong You[4]

[1]Biomedical Electronic Engineering Program
Faculty of Electronic Engineering and Technology, Universiti Malaysia Perlis, Pauh Putra Campus, 02600 Arau, Perlis, Malaysia
[2]Medical Device and Life Science Cluster, Sport Engineering Research Centre (SERC) Universiti Malaysia Perlis, Pauh Putra, 02600 Arau, Perlis, Malaysia
[3]Manufacturing and Materials Engineering Department, Kulliyyah Engineering, International Islamic University Malaysia (IIUM), Jalan Gombak, 53100 Kuala Lumpur, Malaysia.
[4]Department of Engineering and Built Environment, Tunku Abdul Rahman University College, 77, Lorong Lembah Permai 3, 11200 Tanjung Bungah, Pulau Pinang

Received 9 July 2022, Revised 4 September 2022, Accepted 8 September 2022

ABSTRACT

Millions of tons of seashells are produced every day as waste around the world. These underutilized seashells waste was executed as calcium precursor by researcher to synthesis the nano-hydroxyapatite (nano-HA). Nano-HA was successfully synthesised from Pholas Orientalis seashells waste via the chemical precipitation method. Different sintering temperatures were implemented to evaluate the physicochemical criteria of nano-HA. The obtained powders were examined by various physicochemical methods such as XRD, FTIR, FESEM, EDX and degradation analysis. The peaks in XRD and FTIR analysis the HA is successfully produced. The FESEM images on the other hand showing the HA particle in nano size range with rice-like structure. Meanwhile, a variation of Ca/P ratio can be observed in respect to sintering temperatures. The Ca/P ratio for HA-WS, HA-S500 and HA-S700 sample is 1.78, 2.03 and 1.57 respectively. Different sintering temperatures result in different crystallinity value which consequently affects its degradation profile.

Keywords: Nano-Hydroxyapatite, Pholas Orientalis seashells and degradation analysis

1. INTRODUCTION

Hydroxyapatite (HA) with chemical formula of $Ca_{10}(PO_4)_6(OH)_2$ is a major component of bone and widely used in biomedical application [1]. The lattice structure is hexagonal with lattice parameters of a=b=9.432Å and c=6.881Å [2]. HA is a bioactive, biocompatible and osteoconductive material which assists the osteosynthesis process when implanted due to the good compatibility and similar composition to the natural bone [3]. Due to its huge application prospects, a lot of researches have been made in demand to synthesised HA with more practical methods by using seashells' waste as a calcium precursor [4]. As seashells composed a high amount of calcium carbonate ($CaCO_3$) [5], seashells have a great possibilities to become a calcium precursor in synthesising the HA. In addition, seashells is still underutilized and considered as waste which dumped into landfills without any post treatment [6]. This material are accessible for the conversion to calcium oxide (CaO) or calcium hydroxide ($Ca(OH)_2$) which exhibit the easiness for utilization [7]. Not only that, due to the expensive price of HA [8], the execution of HA based on waste materials is highly interesting [9].

*nashrul@unimap.edu.my

Based on the previous reports, HA based on this biogenic resources yield different properties such as its purity and morphologies [9]–[11]. Pholas Orientalis is the scientific name for angel wing clam. It is a marine bivalve seashells found in Asian countries such as Japan, India, Philippines and Malaysia [12]. Locally, Pholas Orientalis is known as "Siput Mentarang" and can be numerously available in Kuala Perlis, Kuala Kedah and Selangor shorelines [13]. Pholas Orientalis is a seashell that consists of two elongated shells that are fixed on a flexible ligament that can be found buried in compact muddy sand [14].

To the best of our knowledge, the implementation of Pholas Orientalis shells waste as the calcium precursor to synthesis the nano HA is still scarce. HA have been synthesised via several routes such as sol gel method [15], micro emulsion method [16], hydrothermal method [17] and combination methods [18] and precipitation method [19]. Chemical precipitation imposed a few advantages such as simplicity, low reaction time and temperatures, high purity and cost effectiveness [20]–[22]. Among all methods, chemical precipitation method is one promising method to produce nano size particles [23]–[25]. This is because the adjustment in synthesis temperature and pH value could manipulate the particle sizes [25]. Practically, nano size HA manifest a good protein adsorption, osteoblast adhesion [26] and good bioactivity [27], [28]. This because the nano size HA particles could improve the bioactivity and biocompatibility [29]. A progressive research are needed for a biocompatible materials having similar composition with human body in nanoscale range [30].

For some application, crystallinity is importance to ensure better performance when implanted. For instance, low crystallinity of HA in coating application for implants is unfavourable for biomedical application. The low crystallinity of HA may hasten the speed of dissolution and this is detrimental for bone bonding at early stage of implantation [31]. Higher crystallinity of HA can be achieved by sintering the HA [32]. Literally, sintering work will affect the crystal grain size of the HA particles [33] and consequently its degradation rate [34]. Specifically, a higher dissolution rate is possessed by the nano size HA. Nano size HA consists a lot of boundaries whereby the dissolution process easily take place at the grain boundaries [35]. The solubility on the other hand is also affected by the low crystallinity and Ca/P ratio [36], [37]. Prakasam et al., claimed that the reports studying the effect of chemical components and stoichiometry HA upon its degradation is still limited [38]. In this study, Pholas Orientalis (Mentarang) seashells were used to synthesise the nano HA by using wet precipitation method. The nano HA were synthesised at three different sintering temperature which are 0°C (not sintered), 500°C and 700°C. These synthesised nano HA's were then undergo several analyses which are X-Ray Diffraction (XRD), Fourier Transform Infrared (FTIR), Field Emission Scanning Electron Microscopy (FESEM), Energy Dispersive X-Ray (EDX) and degradation analysis.

2. MATERIAL AND METHODS

2.1 Synthesis of HA powder

Seashell's waste based on Mentarang (Pholas Orientalis) was collected and further purified. Initially, the seashells were boiled in distilled water at 100°C to remove any dirt or flesh. Then, the seashells were dried in an oven dryer for 1 hour at 100°C before it is crushed into powder form by using a grinder. At this stage, the seashells powder is comprised of calcium carbonate ($CaCO_3$) and then heated at 1100°C with the rate of 10°C/min by using furnace. The heating of

$CaCO_3$ powder would convert it into calcium oxide (CaO) powder. Next, the CaO powder was measured to be 5g and immersed in 500ml distilled water (H_2O) for 24hours. By mixing both CaO and H_2O materials, calcium hydroxide ($Ca(OH)_2$) was formed as the product. To ensure a complete formation of $Ca(OH)_2$, after mixing for 24hours, the solution was stirred using magnetic stirrer at 500rpm under 45°C for 2hours. After 2hours, 2.8ml of phosphoric acid (H_3PO_4) was added into the solution at rate 0.1ml/min. In this work, calcium precursor is derived from seashells waste ($CaCO_3$) while phosphate precursor from H_3PO_4. Both precursors were calculated to be 1.67 which subjected to Ca/P ratio of HA. While adding the H_3PO_4 in the solution, the pH of the solution was monitored and adjusted to pH11 by dropping ammonia (NH_3). At this stage, the resultant gelatinous solution formed was allowed to age for 24hours under room temperature. The precipitate formed was then filtered and washed with distilled water before drying in oven dryer for 6 hours at 110°C to remove the moisture completely. The HA cake formed previously was then powdered by using mortar and pestle. For the next step, some of the samples undergone the sintering process as sintering temperature is the manipulated variable in this experiment. The powder undergoes sintering process for 3hours at the rate of 8°C/min. A non-sintering HA sample was labelled as HA-WS while the sintered HA samples at 500°C and 700°C were labelled as HA-S500 and HA-S700 respectively.

2.2 Characterization

2.2.1 X-Ray Diffraction (XRD) Spectrometry

The XRD analysis conducted to analyze the phase and crystallographic of the HA powder. XRD machine model of Brucker D2 Phaser was used to scan the powder. Samples for characterization were prepared by compacting the HA powders in the XRD holder. The scan range was set from 10°C to 90°C with the step size 0.1° and 5°/min of scan rate. The obtained XRD pattern was compared with the X'pert Highscore Plus V.2.2.5 software. The crystallinity phase (X_c) and crystallite size (X_s) were calculated by using Equation 1 and Equation 2 respectively.

$$\text{Crystallinity phase, } X_c = \frac{V_{112/300}}{I_{300}} \quad (1)$$

Where I_{300} is the intensity at 300 reflection and $V_{(112/300)}$ is the intensity of hollow between (120 and (300) diffraction

$$\text{Crystallite size, } X_s = \frac{k\lambda}{FWHM\cos\theta} \quad (2)$$

Where λ is the wavelength of monochromatic X-ray beam (nm) (λ = 0.15406nm for CuKα radiation); FWHM is the full width at half maximum of the diffraction peak under consideration (rad). The diffraction peak at 2θ=25.88° which assign to (002) plane was chosen for calculation of crystallite size since it is sharper and isolated from others.

2.2.2 Fourier Transform Infrared (FTIR) Spectroscopy

Identification and verification of functional group exist in HA powders were done via FTIR analysis. FTIR equipment model of Perkin Elmer Spectrum 65 was set at the frequency spectrum at the range of 400cm^{-1} to 4000cm^{-1}.

2.2.3 Field Emission Scanning Electron Microscopy (FESEM) and Energy Dispersive X-Ray (EDX) spectroscopy

FESEM model of Hitachi was used to examine the morphologies of HA samples with 15kV excitation voltage. Prior to FESEM scanning, HA samples were prepared by dispersing the powder onto the double-sided carbon tape mounted on the aluminum sample holder. Then, the samples were coated with a thin Platinum (Pt) layer before observed under the FESEM. While, EDX on the other hand was performed to examine the elemental compositions in the HA powder.

2.2.4 Degradation analysis

Upon the degradation and the bioactivity analysis, 0.25 gram of HA samples were pressed with a uniaxial press (MSE, MP10, Turkey) of 150 MPa for 30s into 1.6 mm thick and 10 mm diameter pellets as shown in Figure 1.

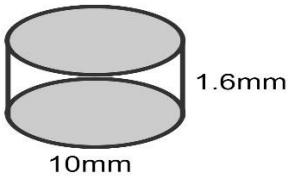

Figure 1. Size of HA pellet for degradation analysis

To conduct this analysis, the HA samples were immersed in phosphate buffered saline (PBS, Merck) solution at pH 7.4 and 37°C for 28 days in the incubator. The PBS solution was not changed within 28 days. To prepare the PBS solution, a plastic beaker was used instead of glass beaker as any scratches from the glass beaker could induce the apatite nucleation on the surface of the beaker [39]. Initially, the PBS tablet was dissolved completely in beaker by using distilled water. After dissolving the PBS tablet, the solution transferred to a volumetric flask and filled with distilled water up to 1 litre to produce 0.1M of PBS solution. To achieve PBS solution with pH7.4, sodium chloride and hydrochloric acid were used to adjust the pH value.

PBS solution was ready once it achieved the pH 7.4. Next, synthesised HA and commercial HA pellets were inserted into respective centrifugal tube by using forceps with vertical position to ensure maximum interaction with the PBS solution. Only then, 10ml of PBS solution is poured into the respective centrifugal tube contained HA pellets. Each centrifugal tubes are then labelled before being kept in the incubator at 37°C over a period of 28 days. After certain periods (0, 7, 14, 21 and 28 days), the pH value of PBS solution was measured, and the samples were removed from the solution to measure its water uptake. After measurement had been made, the samples were kept in the desiccator for 24hours for drying. After 24hours, the measurement was made to quantify the weight loss. Water uptake and weight loss were quantify using Equation 3 and 4 respectively. Finally, the HA samples undergo FESEM to observe the structure and apatite formation on its surface.

$$\text{Water uptake (\%)} = \frac{W_w - W_i}{W_i} \text{x}100\% \quad (3)$$

Ww = Weight of the final sample (after immersion)
Wi = Weight of the initial sample

$$\text{Water loss (\%)} = \frac{W_i - W_f}{W_i} \text{x}100\% \quad (4)$$

Ww = Weight of the final sample (after drying in desiccator)
Wi = Weight of the initial sample

3. RESULTS AND DISCUSSION

3.1 The phase and crystallinity of HA

XRD analysis was done to study the crystallinity and the phase of the HA samples. All the synthesized HA samples show a conventional HA peaks. Figure 2 shows the XRD peaks of commercial HA, HA-WS, HA-S500 and HA-S700. All the peaks show different intensity due to the different sintering temperature. Generally, all peaks are matched and aligned with HA PDF 01-074-0565 file at Miller's plane of (002), (102), (210), (211), (112), (300), (202), (130), (222) and (213) which respect to 26.04°, 28.13°, 28.92°, 31.77°, 32.20°, 32.90°, 34.06°, 39.79°,46.70 and 49.49° respectively. Nevertheless, not all planes can be observed in one HA sample. For instance, (112) plane can be obviously seen for HA-S700 HA and commercial HA but not for HA-S500 and HA-WS. At this plane, this peak is similarly appeared in commercial HA but HA-S700 is more intense and sharper compared to commercial HA. HA-S700 sample also has sharper peaks at (002), (102), (210), (130), (222) and (213) compared to the other synthesised HA. This is understood as sintering the HA sample could increase its crystallinity [40] as represented by the sharp peak in XRD analysis.

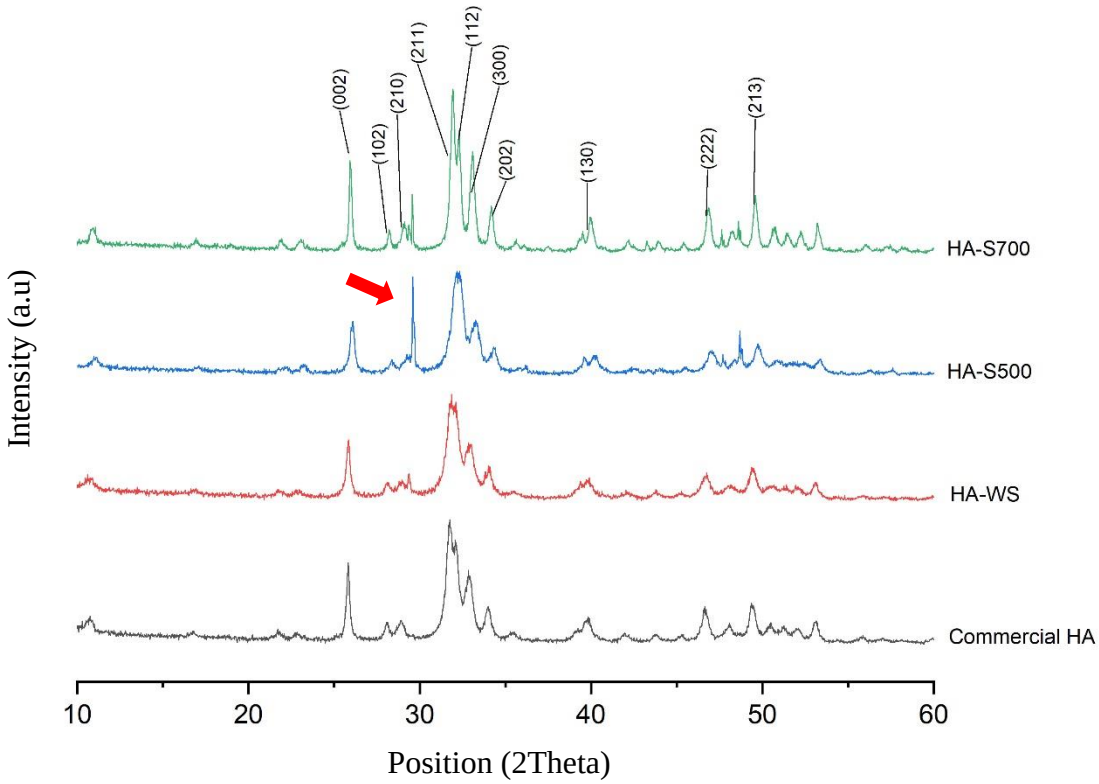

Figure 2. XRD peaks of commercial and synthesized HA

Table 1 shows the crystallite size and its crystallinity for respective HA samples. By sintering the HA sample, the crystallinity will increased as presented in [41], [42] works. However, this phenomenon is contradicting if comparison is being made between the non-sintering HA (HA-

WS) and sintering HA at 500°C (HA-S500). The later sample shows a lower crystallinity value compared to non-sintering HA which is 18.58% and 30.75% respectively. HA-S500 sample has lower crystallinity value compared to HA-WS sample might be due to the present of calcite. Calcite is one of the $CaCO_3$ phase [43] present at 29.42° (JCPDS card No.01-072-1650) in XRD spectrum as shown in Figure 2 labelled with red arrow. As mentioned before, the presence CO_3^{2-} will cause low crystallinity and restrict the crystal growth [6].

Practically, this calcite peak can be observed in HA-WS sample with less intense peak but getting sharper and intense as the sample sintered at 500°C (HA-S500). This is due to the optimum temperature for calcite occurrences is 500°C and decomposed at the temperature more than 600°C [44]. Hence, for the HA sample sintered at 700°C (HA-S700), the calcite peak shows less intense peak imposed when the calcite has been decomposed. Theoretically, the cell dimension of conventional HA at a and b axis is 0.9418nm while c axis is 0.6884nm [45]. From Table 1, the a and c lattice parameter for all samples are nearly approaching the lattice parameter of conventional HA. The deviation of lattice parameter a is greater compared to c which show a small fluctuation from the standard value of HA. This mainly due to the substitution of CO_2^{-3} ions which has lower ionic radius replacing PO_4^{3-} ions with higher ionic radius. Introduction of lower ionic radius developed a distortion at a-axis channel especially for HA-S500 and HA-S700 samples.

Table 1. Calculation of lattice parameter, crystallite size and crystallinity of HA at different sintering temperature

Sample/Parameter	Lattice parameter (nm)		Crystallite size, X_s (nm)	Crystallinity, X_c (%)
	a	c		
Commercial HA	0.943	0.690	125.49	58.81
HA-WS	0.943	0.689	94.12	30.75
HA-S500	0.937	0.683	75.33	18.58
HA-S700	0.938	0.687	107.62	50.13

3.2 FTIR analysis on the HA samples

Figure 3 shows the comparison of FTIR spectrum among all the HA samples. For all samples, they show a common functional group of OH and PO_4^{3-} which confirms the formation of HA [46]. The PO_4^{3-} group for all samples can be observed at 962cm^{-1} and 1036cm^{-1} [29]. But for samples sintered at 700°C, this peak shows a new growth peak at 1090cm^{-1} which is considered as an additional marker for HA [47]. For all samples, peak at 1740cm^{-1} was observed which refers to the stretching of carbonyl compound. This compound actually belongs to amide group which derived from NH_4OH that has been used during synthesising process while adjusting the pH value.

In all samples, carbonate (CO_3^{2-}) functional group can be found with low intensity at peak 874cm^{-1} and 1419cm^{-1}. Thereby, this suggest that all the synthesised HA are carbonated HA type B [48], [49]. For the carbonated HA type B, it is understood that the CO_3^{2-} ions are substituted by PO_4^{3-} ions in HA lattice [49]. CaO peak on the other hand can be found at 667cm^{-1} for all HA samples.

For the non-sintering HA sample (HA-WS), this peak is more obvious compared to the sintering HA samples (HA-S500 and HA-S700). By increasing the sintering temperature will reduce the intensity of the CaO peak. It is suggested that CaO was presented in the non-sintering sample due to the oxygen from the environment dissolved during the synthesising process. Meanwhile, CaO was presented in the sample sintered at 700°C as a minor phase due to the sintering process and this finding is similar as reported by Phatai et al., [50]. Thus, it is understood that sintering of the HA samples could manipulate the existence of CaO and CO_3^{2-}.

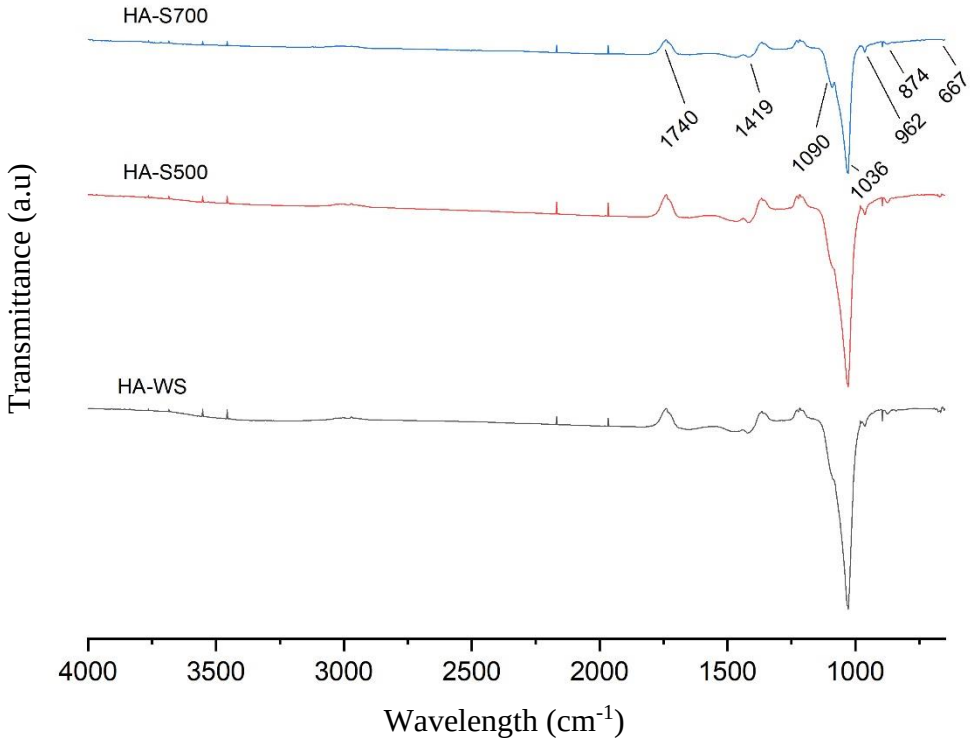

Figure 3. FTIR spectrum of HA samples

3.3 The evaluation on morphology and Ca/P ratio

From the FESEM images in Figure 4, Figure 5 and Figure 6, they show that all samples have a rice like particle structure with nanometre size. The dimension of each particle in term of its length and width are shown in Table 2. Basically, all the samples have particles size ranging from 1nm to 100nm± which favourable for degradation and bioactivity [51]. From Table 2, it shows that the length of HA particles had increased when sintering work was implemented on the HA samples. The nucleation might take place when high temperature is applied which result the length growing. The non-sintering HA sample (HA-WS) has the smallest dimension (length and width) compared with others sintering HA samples. This particularly caused by the CO_3^{2-} contents which limits the crystal growth [6], [52], [53].

FESEM analysis was performed to examine the morphology of HA samples. From the FESEM images, it can be observed that sintering temperature could affect the agglomeration in HA samples. Sintering the HA samples in [54], [55] works show an agglomeration on the HA

structures. While in this work, the non-sintering HA sample (HA-WS) shows a higher number of agglomeration and big clump on the HA structure as shown in Figure 4 marked with the red circle. This phenomenon might happen due to incomplete conversion of CaO to $Ca(OH)_2$ when reacted with distilled water at the early stage of HA synthetisation. This unreacted CaO later on reacted with the carbon dioxide (CO_2) from the surrounding during HA synthesis which consequently produced CO_3^{2-}. Hence, during the synthesis of HA-WS sample, there are a lot of active ions such as CO_3^{2-}, PO_4^{3-}, OH^- and Ca^{2+}. A big number of active ions interacting with each other raised a higher attraction between the ions subsequently increased the agglomeration tendency in HA. This is the reason for the big clumps and agglomerations can be seen in HA-WS sample. Agglomeration still occur in HA-S500 and HA-S700 but not too obvious as imposed in HA-WS sample. The agglomeration is marked with the red circle as shown in Figure 5 and Figure 6.

The EDX spectra is shown in Figure 7, Figure 8 and Figure 9. In the EDX spectra, major elements such as Ca, P, and O in the HA samples are confirmed. C element on the other hand existed due to the presence of CO_3^{2-} and CaO as impurity in HA samples. The Ca/P ratio for HA-WS, HA-S500 and HA-S700 sample is 1.78, 2.03 and 1.57 respectively. The atomic percentage for all elements and Ca/P ratio of all samples were presented in Table 3. The highest Ca/P ratio could be observed for samples HA-WS and HA-S500. The higher Ca/P ratio is owed to the present of CaO [56] and due to the ions substitution such as CO_3^2 in HA lattice structure [57]. The higher value of Ca/P ratio for HA-WS and HA-S500 samples is claimed due to the content of secondary phase such as CaO or CO_3^{2-}. This can be justified by referring to C atomic percentage in Figure 7 and Figure 8. As the secondary phase is higher in HA-WS and HA-S500 samples, the atomic percentage of C element shows the highest value compared to HA-S700 samples.

Table 2. The dimension of HA particle

Dimension/Sample	HA-WS	HA-S500	HA-S700
Length (nm)	161.609	184.312	187.359
Width (nm)	158.953	172.941	170.801

Table 3. The atomic percentage and Ca/P ratio of all HA samples

Sample / Element	Atomic percentage (at%)				Ca/P ratio
	C	O	P	Ca	
HA-WS	48.49	38.48	4.68	8.35	1.78
HA-S500	50.65	33.53	5.22	10.60	2.03
HA-S700	20.69	58.72	8.00	12.59	1.57

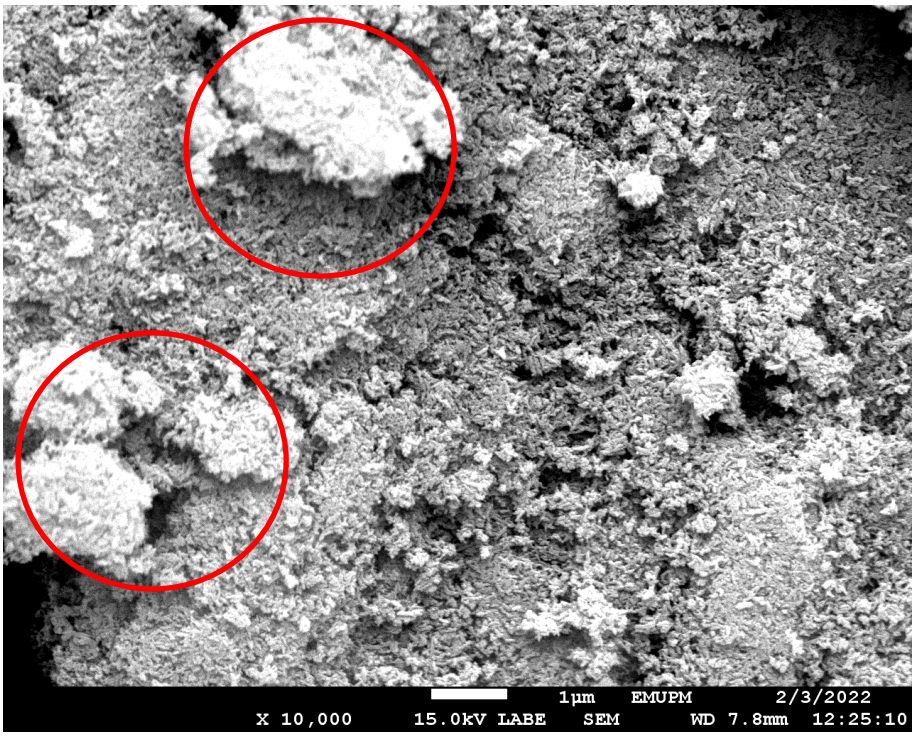

Figure 4. FESEM image of HA-WS sample with agglomeration marked with red circle

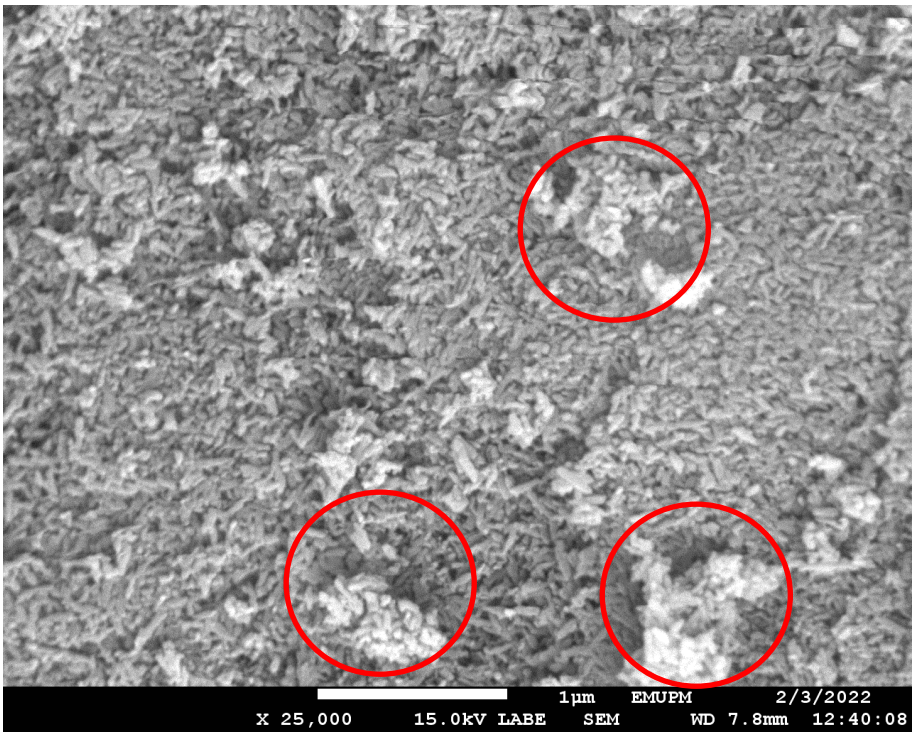

Figure 5. FESEM image of HA-S500 sample with agglomeration marked with red circle

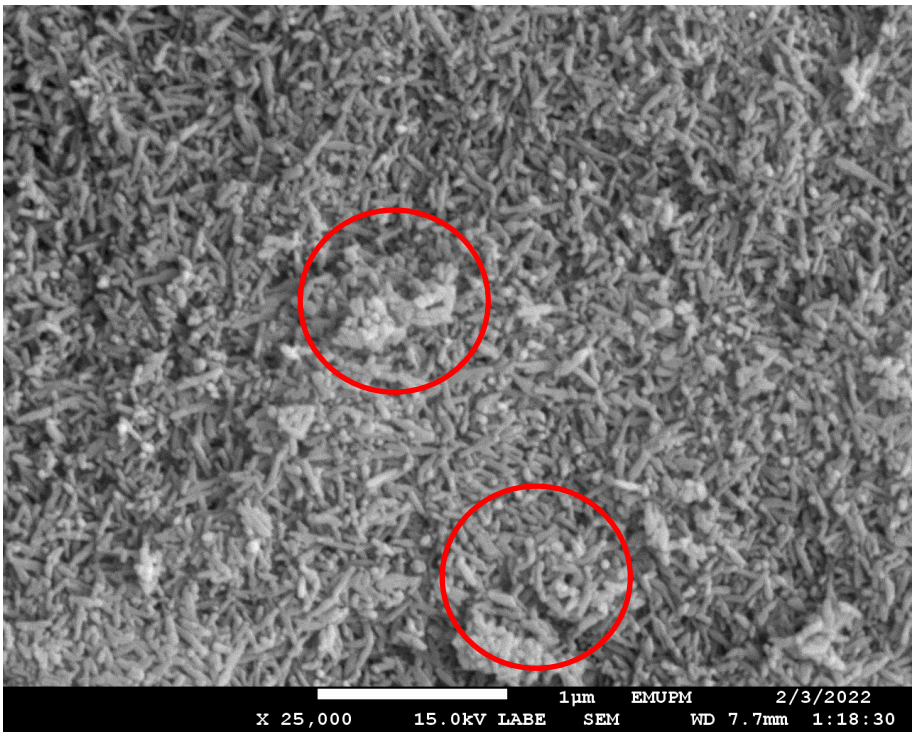

Figure 6. FESEM image of HA-S700 sample with agglomeration marked with red circle

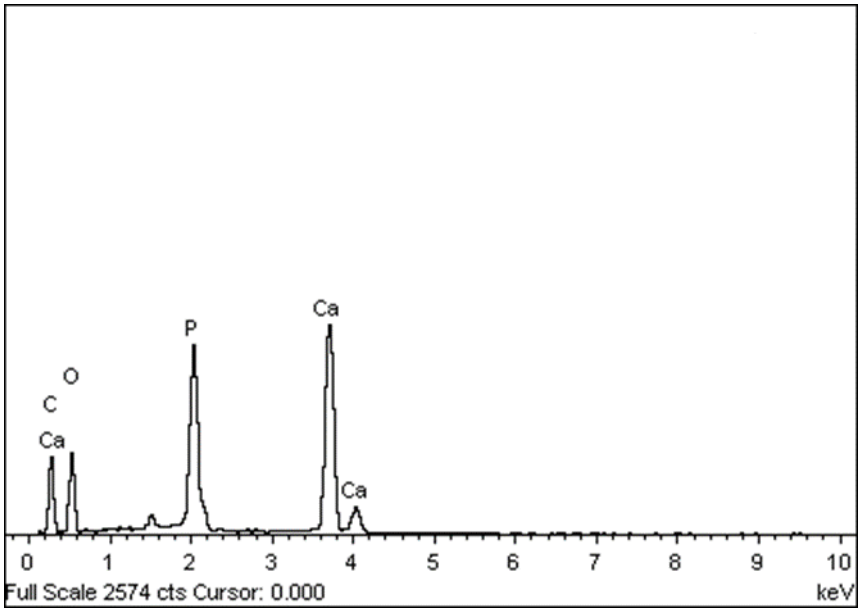

Figure 7. EDX spectra for HA-WS sample

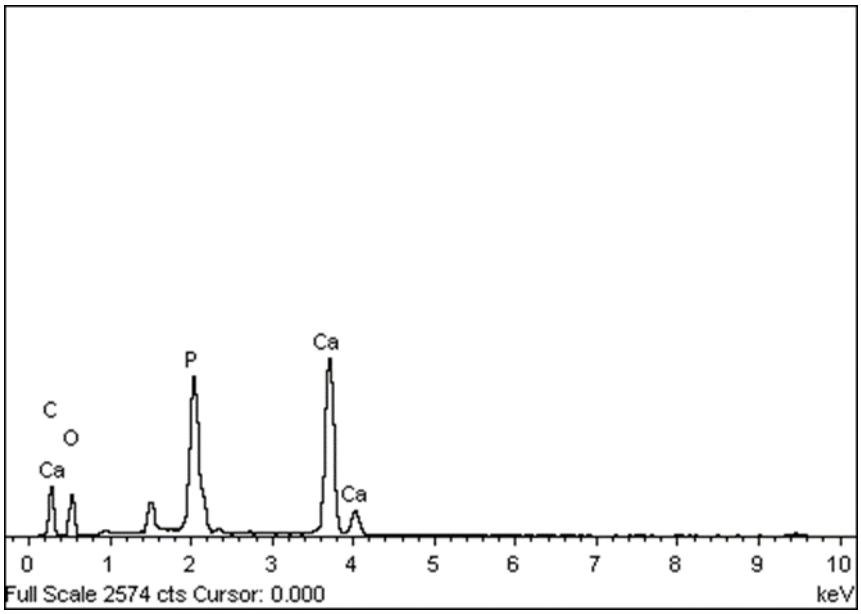

Figure 8. EDX spectra for HA-S500 sample

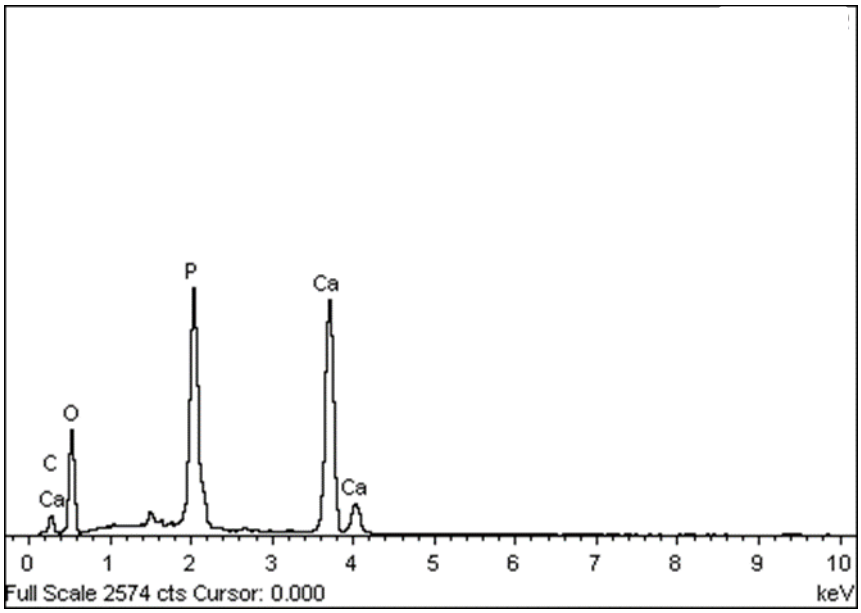

Figure 9. EDX spectra for HA-S700 sample

3.4 The biodegradation study

In vitro of degradation analysis was done upon synthesised and commercial HA. Figure 10 shows the pH changes when all the HA samples were immersed in PBS solution. PBS solution is a buffer medium that reduces the drastic changes in acid or base environment. Overall, pH of the SBF solution increased after 7th day of immersion. However, PBS medium of HA-500 shows a higher increment compared to the other samples. Theoretically, an increment of pH value is due to the CaO content. After immersion, the CaO content in HA samples were dissolved in PBS solution and released Ca^{2+} ions. This ion subsequently reacted with the PBS medium to form ($Ca(OH)_2$) and

gave a rise to the pH value. Hence, it can be concluded that the HA-S500 sample composed a higher CaO content followed by HA-S700 and HA-WS sample. Commercial HA on the other hand shows small change in its pH value after 7th day of immersion. This probably due the nature of pure HA which is less soluble [58] hence Ca^{2+} released at lower rate and gave a small rise in pH value. After 7th days of immersion, all the samples show a decrement trend it its pH value up to 21st day. This is possibly due to amount of CaO getting lesser along the 21st thereby less affects to the pH value. Nevertheless, the synthesised HA samples on 28th day show a pH rising. During this period, a rush dissolution of Ca^{2+} ions might have started again from the newly apatite formation and gave a rise to its pH value.

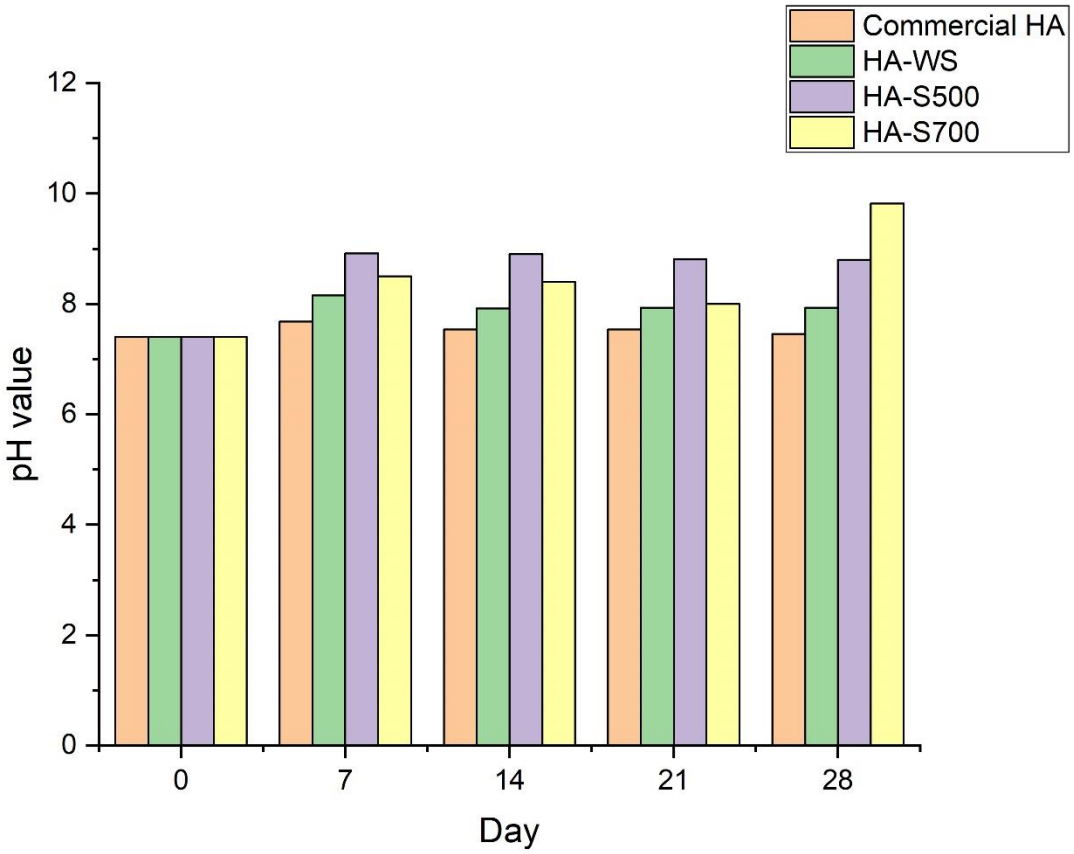

Figure 10. pH changes in PBS medium

The water uptake was increased after the 7th day of immersion for all synthesised HA samples. This implies that the absorption rate is good for all samples and the water uptake was executed by the binding of both Ca^{2+} and OH^- ions from HA sample and PBS medium itself. After the 7th days, water uptake was reduced for HA-WS and HA-S500 samples up to the 28th day. For HA-S700 sample, the water uptake occurred only up to the 21st day. The water uptake was reduced due to the less capability of the sample to absorb and to trap the water molecule as the samples degraded. Contrarily, as for HA-S700 sample, the water uptake had risen again from the 21st day to the 28th day. This phenomenon may due to the new apatite formation and this had increased the binding of Ca^{2+} and OH^- ions. Thus, consequently increased the water uptake again. Aforementioned, a low crystallinity of HA will increase the rate of dissolution [31]. As the HA-S500 has the lowest crystallinity among all, the water uptake had drastically decreased at the 28th

day. Herein, it is believed that the sample had dissolved and degraded extensively, hence reducing the water uptake.

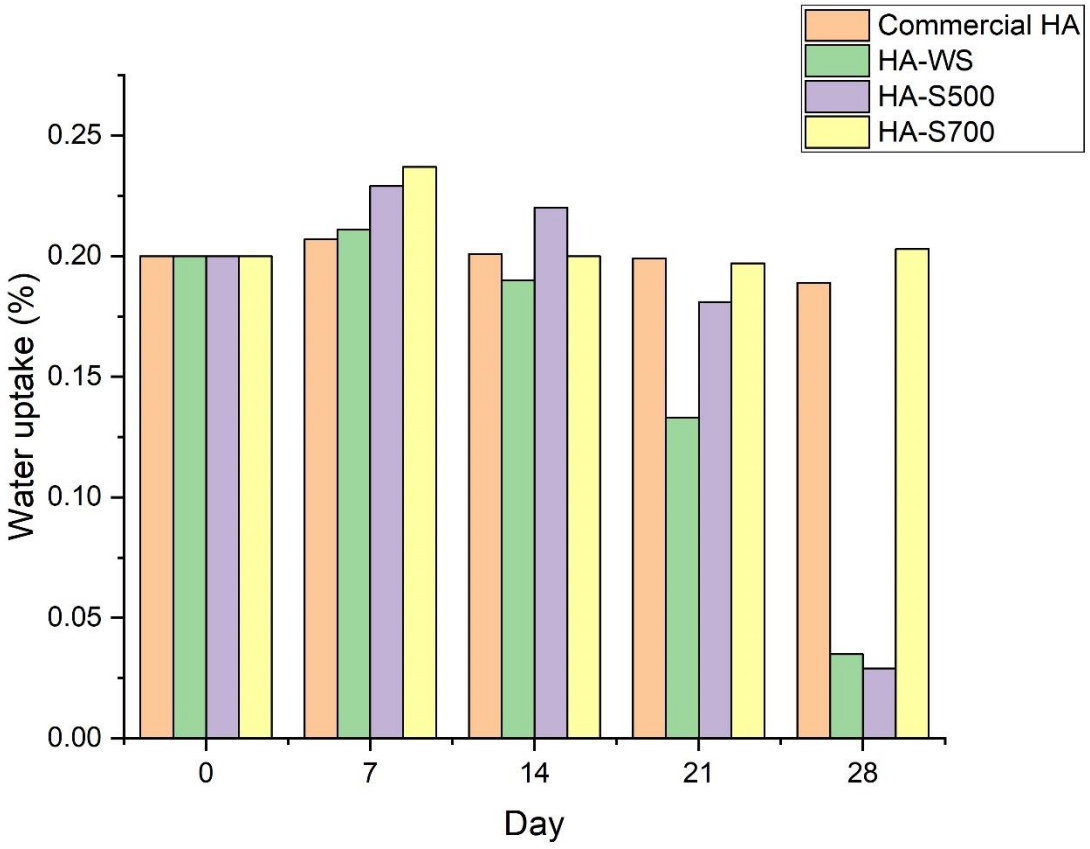

Figure 11. Water uptake (%) in PBS medium

The weight loss of synthesised HA (HA-WS and HA-S500) samples in PBS medium from the 7th day to the 28th day showed an incremental trend. As the samples were composed of CaO as impurity, they were easily dissolved when immersed in the PBS solution and accelerated the weight loss which consequently facilitate the degradation rate. In contrast to HA-S700 sample, the weight loss is drastic from the 7th day until the 21st day. On the 28th day, the weight loss was slower but the degradation is still happened. This phenomenon results in more Ca+ dissolute into the medium to favors the apatite formation. Hence, the new apatite may take place hence the less weight loss could be observed within this period.

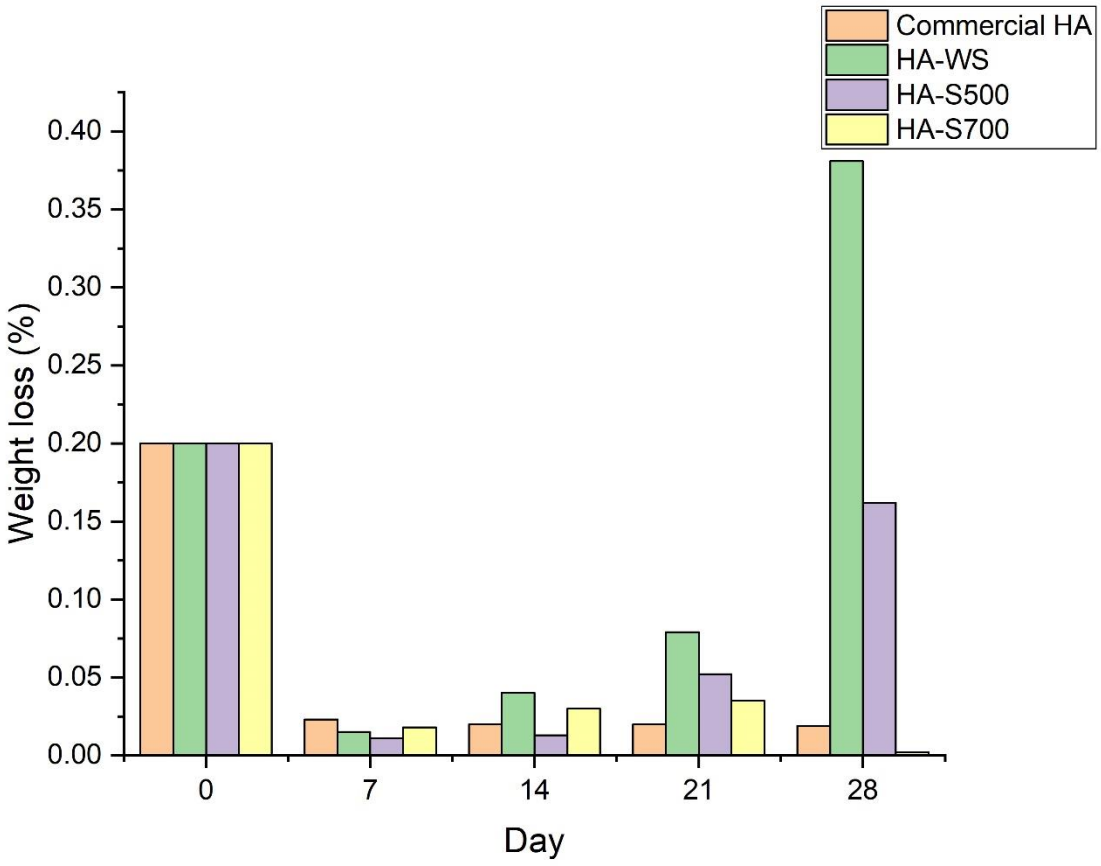

Figure 12. Weight loss in PBS medium

4. CONCLUSION

As the conclusion, nano HA can be synthesized from shells of Pholas Orientalis (Mentarang) via chemical precipitation method. The conventional HA peaks can be observed from XRD analysis. The calculation of crystallite size and crystallinity percentage showed a variation values when sintering temperature was manipulated. A higher crystallinity can be observed for HA samples undergone sintering process. This consequently affects the degradation profile whereby the lowest crystallinity causes a greater degradation. FTIR analysis on the other hand shows a common chemical compound of HA with some impurities while FESEM analysis confirmed the HA in nano scale range. The impurities cause the deviation in Ca/P ratio which characterized by EDX analysis.

ACKNOWLEDGEMENTS

Our greatest appreciation goes to Faculty of Electronic Engineering Technology (Biomaterials Laboratory) UniMAP, Faculty of Chemical Engineering Technology, Universiti Malaysia Perlis and Microscopy Unit, Biosciences Institute, Malaysia Putra University. This work was supported by Research Materials Fund (RESMATE, 9001-00626) from University Malaysia Perlis.

REFERENCES

[1] B. A. E. Ben-Arfa, I. M. M. Salvado, J. R. Frade, and R. C. Pullar, "Fast route for synthesis of stoichiometric hydroxyapatite by employing the Taguchi method," *Mater. Des.*, vol. 109, pp. 547–555, Nov. 2016.

[2] W.-F. Ho, H.-C. Hsu, S.-K. Hsu, C.-W. Hung, and S.-C. Wu, "Calcium phosphate bioceramics synthesized from eggshell powders through a solid state reaction," *Ceram. Int.*, vol. 39, no. 6, pp. 6467–6473, Aug. 2013.

[3] U. Anjaneyulu, U., Pattanayak, D. K., & Vijayalakshmi, "The facile and phase pure evaluations of nano hydroxyaptite powder by sol-gel method," *Int. J. ChemTech Res*, vol. 7, pp. 1516–1520, 2014.

[4] D. Ulfyana, F. Anugroho, S. H. Sumarlan, and Y. Wibisono, "Bioceramics synthesis of hydroxyapatite from red snapper fish scales biowaste using wet chemical precipitation route," *IOP Conf. Ser. Earth Environ. Sci.*, vol. 131, no. 1, 2018.

[5] E. Barua, A. B. Deoghare, P. Deb, and S. Das Lala, "Naturally derived biomaterials for development of composite bone scaffold: A review," *IOP Conf. Ser. Mater. Sci. Eng.*, vol. 377, p. 012013, Jun. 2018.

[6] S. H. Saharudin, J. H. Shariffuddin, A. Ismail, and J. H. Mah, "Recovering value from waste: biomaterials production from marine shell waste," *Bull. Mater. Sci.*, vol. 41, no. 6, p. 162, Dec. 2018.

[7] I. Fatimah, G. R. Aulia, W. Puspitasari, R. Nurillahi, L. Sopia, and R. Herianto, "Microwave-synthesized hydroxyapatite from paddy field snail (Pila ampullacea) shell for adsorption of bichromate ion," *Sustain. Environ. Res.*, vol. 28, no. 6, pp. 462–471, Nov. 2018.

[8] P. Tempesti, G. S. Nicotera, M. Bonini, E. Fratini, and P. Baglioni, "Poly(N-isopropylacrylamide)-hydroxyapatite nanocomposites as thermoresponsive filling materials on dentinal surface and tubules," *J. Colloid Interface Sci.*, vol. 509, pp. 123–131, Jan. 2018.

[9] D. Núñez, E. Elgueta, K. Varaprasad, and P. Oyarzún, "Hydroxyapatite nanocrystals synthesized from calcium rich bio-wastes," *Mater. Lett.*, vol. 230, pp. 64–68, Nov. 2018.

[10] M. Akram, R. Ahmed, I. Shakir, W. A. W. Ibrahim, and R. Hussain, "Extracting hydroxyapatite and its precursors from natural resources," *J. Mater. Sci.*, vol. 49, no. 4, pp. 1461–1475, Feb. 2014.

[11] M. Sadat-Shojai, M.-T. Khorasani, E. Dinpanah-Khoshdargi, and A. Jamshidi, "Synthesis methods for nanosized hydroxyapatite with diverse structures," *Acta Biomater.*, vol. 9, no. 8, pp. 7591–7621, Aug. 2013.

[12] J. . Berthou, P., Poutiers, J. M., Goulletquer, P. and Dao, "Shelled molluscs, in fisheries and agricultural," *life support systems (EOLSS)*. Eolss Publ. Oxford, UK, pp. 1–19, 2009.

[13] N. B. Wah, "Biological aspect and development of larvae and juvenile of the angelwing clam P.orientalis (Gmeline, 1971)," 2009.

[14] H. bt M. Yusop and M. F. S. bin Ramli, "The Study of Pholas Orientalis's Life Cycle and Its Relationship with the Ecological Parameters in States of Kedah, Perak and Selangor, Malaysia," *IOSR J. Agric. Vet. Sci.*, vol. 10, no. 06, pp. 15–20, Jun. 2017.

[15] B. A. E. Ben-Arfa, I. M. M. Salvado, J. M. F. Ferreira, and R. C. Pullar, "Novel route for rapid sol-gel synthesis of hydroxyapatite, avoiding ageing and using fast drying with a 50-fold to 200-fold reduction in process time," *Mater. Sci. Eng. C*, vol. 70, pp. 796–804, 2017.

[16] F. Foroughi, S. A. Hassanzadeh-Tabrizi, and A. Bigham, "In situ microemulsion synthesis of hydroxyapatite-MgFe2O4 nanocomposite as a magnetic drug delivery system," *Mater. Sci. Eng. C*, vol. 68, pp. 774–779, 2016.

[17] H. Yang, J. Hong, L. Wei, and C. Deng, "Synthesis of hydroxyapatite nanoparticles using surface carboxyl-functionalized carbon dots as template," *Ceram. Int.*, vol. 44, no. 14, pp. 16844–16850, 2018.

[18] X. Ji, Y., Wang, A., Wu, G., Yin, H., Liu, S., Chen, B., & Li, "Synthesis of different sized and porous hydroxyapatite nanorods without organic modifiers and their 5-fluorouracil release performance," *Mater. Sci. Eng. C*, vol. 57, pp. 14–23, 2015.

[19] M. R. Vahabi, H., Shabanian, M., Aryanasab, F., Mangin, R., Laoutid, F., & Saeb, "Inclusion of modified lignocellulose and nano-hydroxyapatite in development of new bio-based adjuvant flame retardant for poly (lactic acid)," *Thermochim. Acta*, no. 666, pp. 51–59, 2018.

[20] V. Rajkumar, M., Sundaram, N. M., & Rajendran, "Preparation of size controlled, stoichiometric and bioresorbable hydroxyapatite nanorod by varying initial pH, Ca/P ratio and sintering temperature," *Dig. J. Nanomater. Biostructures*, vol. 6, no. 1, pp. 169–179, 2011.

[21] N. Y. Mostafa, "Characterization, thermal stability and sintering of hydroxyapatite powders

prepared by different routes," *Mater. Chem. Phys.*, vol. 94, no. 2–3, pp. 333–341, Dec. 2005.

[22] O. F. Er, A. Caglar, B. Ulas, H. Kivrak, and A. Kivrak, "Novel carbon nanotube supported Co@Ag@Pd formic acid electrooxidation catalysts prepared via sodium borohydride sequential reduction method," *Mater. Chem. Phys.*, vol. 241, p. 122422, Feb. 2020.

[23] M. N. Salimi, R. H. Bridson, L. M. Grover, and G. A. Leeke, "Effect of processing conditions on the formation of hydroxyapatite nanoparticles," *Powder Technol.*, vol. 218, pp. 109–118, Mar. 2012.

[24] M. Islam, P. Chandra Mishra, and R. Patel, "Physicochemical characterization of hydroxyapatite and its application towards removal of nitrate from water," *J. Environ. Manage.*, vol. 91, no. 9, pp. 1883–1891, Sep. 2010.

[25] A. F. M. Othman, R., Mustafa, Z., Loon, C. W., & Noor, "Effect of calcium precursors and pH on the precipitation of carbonated hydroxyapatite," *Procedia Chem.*, no. 19, pp. 539–545, 2016.

[26] J. R. Woodard *et al.*, "The mechanical properties and osteoconductivity of hydroxyapatite bone scaffolds with multi-scale porosity.," *Biomaterials*, vol. 28, no. 1, pp. 45–54, Jan. 2007.

[27] S. V. Dorozhkin, "Nanosized and nanocrystalline calcium orthophosphates," *Acta Biomater.*, vol. 6, no. 3, pp. 715–734, 2010.

[28] and R. T. Cai, Yurong, Yukan Liu, Weiqi Yan, Qinghong Hu, Jinhui Tao, Ming Zhang, Zhongli Shi, "Role of hydroxyapatite nanoparticle size in bone cell proliferation," *J. Mater. Chem.*, vol. 17, no. 36, pp. 3780–3787, 2007.

[29] V. Rodríguez-Lugo *et al.*, "Wet chemical synthesis of nanocrystalline hydroxyapatite flakes: effect of pH and sintering temperature on structural and morphological properties," *R. Soc. Open Sci.*, vol. 5, no. 8, p. 180962, Aug. 2018.

[30] G. G. Walmsley *et al.*, "Nanotechnology in bone tissue engineering," *Nanomedicine Nanotechnology, Biol. Med.*, vol. 11, no. 5, pp. 1253–1263, Jul. 2015.

[31] D. Liu, K. Savino, and M. Z. Yates, "Coating of hydroxyapatite films on metal substrates by seeded hydrothermal deposition," *Surf. Coatings Technol.*, vol. 205, no. 16, pp. 3975–3986, May 2011.

[32] A. A. Ramesh, S., Loo, Z.Z., Tan, C.Y., Chew, W.K., Ching, Y.C., Tarlochan, F., Chandran, H., Krishnasamy, S., Bang, L.T. and Sarhan, "Characterization of biogenic hydroxyapatite derived from animal bones for biomedical applications," *Ceram. Int.*, vol. 44, no. 9, pp. 10525–10530, 2018.

[33] R. K. Chadha, A. P. Singh, K. L. Singh, C. Sharma, and V. Naithani, "Influence of microwave processing and sintering temperature on the structure and properties of Sr/Zr doped hydroxyapatite," *Mater. Chem. Phys.*, vol. 223, pp. 319–324, Feb. 2019.

[34] N. Prasasti, R. W., Hariyanto, Y. A., & Hidayat, "The Influence of Chitosan Concentration on Synthesis of Hydroxyapatite Scaffold on Crystallinity and Surface Morphology," in *IOP Conference Series: Materials Science and Engineering*, 2018, p. 012024.

[35] K. Lin *et al.*, "Evaluation of host inflammatory responses of β-tricalcium phosphate bioceramics caused by calcium pyrophosphate impurity using a subcutaneous model," *J. Biomed. Mater. Res. Part B Appl. Biomater.*, vol. 99B, no. 2, pp. 350–358, Nov. 2011.

[36] A. L. BURNETT, A. G. CHANG, J. K. CRONE, P. L. HUANG, and S. F. SEZEN, "Noncholinergic Penile Erection in Mice Lacking the Gene for Endothelial Nitric Oxide Synthase," *J. Androl.*, vol. 23, no. 1, pp. 92–97, Jan. 2002.

[37] S. Overgaard, U. Bromose, M. Lind, C. Bünger, and K. Søballe, "The influence of crystallinity of the hydroxyapatite coating on the fixation of implants," *J. Bone Joint Surg. Br.*, vol. 81-B, no. 4, pp. 725–731, Jul. 1999.

[38] M. Prakasam, J. Locs, K. Salma-Ancane, D. Loca, A. Largeteau, and L. Berzina-Cimdina, "Fabrication, Properties and Applications of Dense Hydroxyapatite: A Review," *J. Funct. Biomater.*, vol. 6, no. 4, pp. 1099–1140, Dec. 2015.

[39] T. Kokubo and H. Takadama, "How useful is SBF in predicting in vivo bone bioactivity?," *Biomaterials*, vol. 27, no. 15, pp. 2907–2915, May 2006.

[40] B. Yedekçi, A. Tezcaner, A. Z. Alshemary, B. Yılmaz, T. Demir, and Z. Evis, "Synthesis and sintering of B, Sr, Mg multi-doped hydroxyapatites: Structural, mechanical and biological characterization," *J. Mech. Behav. Biomed. Mater.*, vol. 115, p. 104230, Mar. 2021.

[41] D. O. Obada, E. T. Dauda, J. K. Abifarin, D. Dodoo-Arhin, and N. D. Bansod, "Mechanical properties of natural hydroxyapatite using low cold compaction pressure: Effect of sintering temperature," *Mater. Chem. Phys.*, vol. 239, p. 122099, Jan. 2020.

[42] R. A. Youness, M. A. Taha, H. Elhaes, and M. Ibrahim, "Preparation, Fourier Transform Infrared Characterization and Mechanical Properties of Hydroxyapatite Nanopowders," *J. Comput. Theor.*

Nanosci., vol. 14, no. 5, pp. 2409–2415, May 2017.

[43] and U. V. U. Anjaneyulu, Deepak K. Pattanayak, "Snail Shell Derived Natural Hydroxyapatite: Effects on NIH-3T3 Cells for Orthopedic Applications," *Mater. Manuf. Process.*, vol. 31, no. 2, pp. 206–216, 2016.

[44] H. Sabeur, G. Platret, and J. Vincent, "The effect of ageing and heat treatment on microstructure evolution of a commercial cement paste," *Heat Mass Transf.*, vol. 53, no. 8, pp. 2609–2626, Aug. 2017.

[45] Z. Liu, R., Qiao, W., Huang, B., Chen, Z., Fang, J., Li, Z., & Chen, "Fluorination enhances the osteogenic capacity of porcine hydroxyapatite," *Tissue Eng. Part A*, vol. 24, no. 15–16, 2018.

[46] D. Walczyk, D. Malina, M. Krol, K. Pluta, and A. Sobczak-Kupiez, "Physicochemical characterization of zinc-substituted calcium phosphates," *Bull. Mater. Sci.*, vol. 39, no. 2, pp. 525–535, Apr. 2016.

[47] G. Orilisi *et al.*, "Effect of a Sodium Fluoride-Releasing Rubber Cup on Hydroxyapatite Crystallinity of Human Enamel: FTIR Spectroscopy Analysis," *Dent. Res. Oral Heal.*, vol. 03, no. 01, 2020.

[48] J. G. Amaral, J. P. Pessan, J. A. S. Souza, J. C. S. Moraes, and A. C. B. Delbem, "Cyclotriphosphate associated to fluoride increases hydroxyapatite resistance to acid attack," *J. Biomed. Mater. Res. Part B Appl. Biomater.*, vol. 106, no. 7, pp. 2553–2564, Oct. 2018.

[49] M. Šupová, "Substituted hydroxyapatites for biomedical applications: A review," *Ceram. Int.*, vol. 41, no. 8, pp. 9203–9231, Sep. 2015.

[50] P. Phatai, C. M. Futalan, S. Kamonwannasit, and P. Khemthong, "Structural characterization and antibacterial activity of hydroxyapatite synthesized via sol-gel method using glutinous rice as a template," *J. Sol-Gel Sci. Technol.*, vol. 89, no. 3, pp. 764–775, Mar. 2019.

[51] M. Du, J. Chen, K. Liu, H. Xing, and C. Song, "Recent advances in biomedical engineering of nano-hydroxyapatite including dentistry, cancer treatment and bone repair," *Compos. Part B Eng.*, vol. 215, p. 108790, Jun. 2021.

[52] I. R. Gibson and W. Bonfield, "Novel synthesis and characterization of an AB-type carbonate-substituted hydroxyapatite," *J. Biomed. Mater. Res.*, vol. 59, no. 4, pp. 697–708, Mar. 2002.

[53] G. Muralithran and S. Ramesh, "The effects of sintering temperature on the properties of hydroxyapatite," *Ceram. Int.*, vol. 26, no. 2, pp. 221–230, Mar. 2000.

[54] M. I. Ramli *et al.*, "Effect of sintering parameters on physical and mechanical properties of powder injection moulded stainless steel-hydroxyapatite composite," *PLoS One*, vol. 13, no. 10, p. e0206247, Oct. 2018.

[55] A. Rogina, I. Košić, M. Antunović, M. Ivanković, and H. Ivanković, "The bioactivity of titanium-cuttlefish bone-derived hydroxyapatite composites sintered at low temperature," *Powder Metall.*, vol. 63, no. 4, pp. 300–310, Aug. 2020.

[56] N. A. S. Mohd Pu'ad, P. Koshy, H. Z. Abdullah, M. I. Idris, and T. C. Lee, "Syntheses of hydroxyapatite from natural sources," *Heliyon*, vol. 5, no. 5, p. e01588, May 2019.

[57] S. M. Londoño-Restrepo, C. F. Ramirez-Gutierrez, A. del Real, E. Rubio-Rosas, and M. E. Rodriguez-García, "Study of bovine hydroxyapatite obtained by calcination at low heating rates and cooled in furnace air," *J. Mater. Sci.*, vol. 51, no. 9, pp. 4431–4441, May 2016.

[58] I. Roohani, S. Cheong, and A. Wang, "How to build a bone? - Hydroxyapatite or Posner's clusters as bone minerals," *Open Ceram.*, vol. 6, p. 100092, Jun. 2021.